Proc., Geotechnical Earthquake Engineering and Soil Dynamics V, Geotechnical Special Publication 290, S. J. Brandenberg and M. T. Manzari, eds., ASCE, 626-636.

Volumetric strains from inverse analysis of pore pressure transducer arrays in centrifuge models

Kathleen M. Darby, M.ASCE,[1] Ross W. Boulanger, F.ASCE,[2] and Jason T. DeJong, M.ASCE[3]

[1]Department of Civil and Environmental Engineering, University of California, Davis, 1 Shields Ave, Davis, CA 95616; email: kdarby@ucdavis.edu
[2]Department of Civil and Environmental Engineering, University of California, Davis, 1 Shields Ave, Davis, CA 95616; email: rwboulanger@ucdavis.edu
[3]Department of Civil and Environmental Engineering, University of California, Davis, 1 Shields Ave, Davis, CA 95616; email: jdejong@ucdavis.edu

ABSTRACT

Inverse analyses were used to evaluate the degree of partial drainage occurring during dynamic shaking of liquefying soil profiles in a set of centrifuge model tests. Three tests were performed using the 9-m radius centrifuge at the UC Davis Center for Geotechnical Modeling on saturated Ottawa sand models with initial relative densities of 25, 43, and 80%. Models were subjected to multiple sinusoidal shaking events with acceleration amplitudes ranging from 0.03 to 0.55g. Densely spaced pore pressure transducer arrays provided profiles of pore pressure generation and dissipation; inverse analyses of the pore pressure data were used to obtain volumetric strain profiles during shaking and dissipation. Surface settlements computed by integrating the volumetric strain profiles are compared to surface settlements measured from linear potentiometers. The magnitude of the volumetric strains due to partial drainage and their potential effects on liquefaction responses are discussed.

INTRODUCTION

The response of a potentially liquefiable soil deposit during seismic loading can be strongly affected by the extent and degree to which excess pore water pressures diffuse during and after strong shaking. The degree of partial drainage during earthquake shaking for thick layers of sandy soils (e.g., sands, silty sands, sandy silts) subjected to shorter duration motions is usually small enough that the assumption of fully undrained conditions is reasonable. The degree of partial drainage can increase as the boundaries become more pervious, liquefiable layer thickness decreases, hydraulic conductivities increase, compressibility decreases, and shaking duration increases. Partial drainage during and after strong shaking can be enhanced by installation of drainage elements, which can increase resistance to liquefaction triggering and reduce the deformations that develop after liquefaction triggering (e.g., Howell et al. 2012). The potential

effects of partial drainage have been recognized for decades (e.g., NRC 1985), but remain challenging to quantify for individual case histories or centrifuge model studies.

Centrifuge tests have been used to gain insight into the effects of pore pressure diffusion on liquefaction behaviors through the use of dense sensor arrays within models. Kutter et al. (2008) used dense arrays of pore pressure transducers (PPTs) around a tunnel embedded in liquefiable soil to investigate the mechanisms governing uplift of the tunnel during earthquake shaking. Malvick et al. (2008) and Kamai et al. (2010) used inverse analysis techniques to compute profiles of volumetric strain from densely spaced PPT arrays in centrifuge models designed to investigate void redistribution in sand layers with embedded low-permeability silt layers or overlying low-permeability clay layers.

The present study uses inverse analysis techniques to examine the evolution of volumetric strains due to partial drainage in a set of three saturated, clean sand centrifuge models subjected to multiple shaking events. The three models had an upper layer of Ottawa sand that was placed loose for two models (initial relative density (D_{Ro}) of 43% and 25%) and dense for one model (D_{Ro} of 80%). Densely spaced PPTs provide time histories of pore pressure with depth. Inverse analyses of the PPT data provide profiles of volumetric strain in time. Integration of the volumetric strain profiles provide time histories of surface settlement. The computed settlements are compared to measured surface settlements to confirm the reasonableness of the inverse analysis results. Volumetric strain and partial drainage behaviors in representative shaking events are presented in detail to illustrate their relation to system-level dynamic behaviors. Implications regarding the potential effects of partial drainage on liquefaction triggering or consequences, and the use of these results in ongoing research, are discussed.

CENTRIFUGE MODELS

A set of three centrifuge models were constructed in a flexible shear beam container and tested at the UC Davis Center for Geotechnical Modeling. Models consisted of a 28-cm-thick (model scale) layer of Ottawa sand overlying an 18-cm-thick layer of Monterey sand, overlying a 4-cm-thick gravel saturation layer, as shown in Figure 1. Ottawa sand was placed by dry pluviation at D_{Ro} of 43%, 25%, and 80%, in the three models, respectively. Monterey sand was placed by dry pluviation at D_{Ro} of 85% in all models. Closely spaced vertical arrays of pore pressure transducers (PPT) and accelerometers (ACC) were placed at matching depths throughout the Ottawa sand layer to capture pore pressure generation/dissipation and accelerations throughout the profile; sensors were placed at greater vertical spacing throughout the Monterey sand layer. Sensor locations are provided in the representative cross-section shown in Figure 1. Four linear potentiometers (LP) measured surface settlement. Models were saturated under vacuum with a viscous pore fluid prepared to 20 centistokes (cSt) (model scale) and tested at a centrifuge acceleration of 40g. Results are presented in prototype dimensions based on standard scaling relations for dynamics, unless otherwise noted.

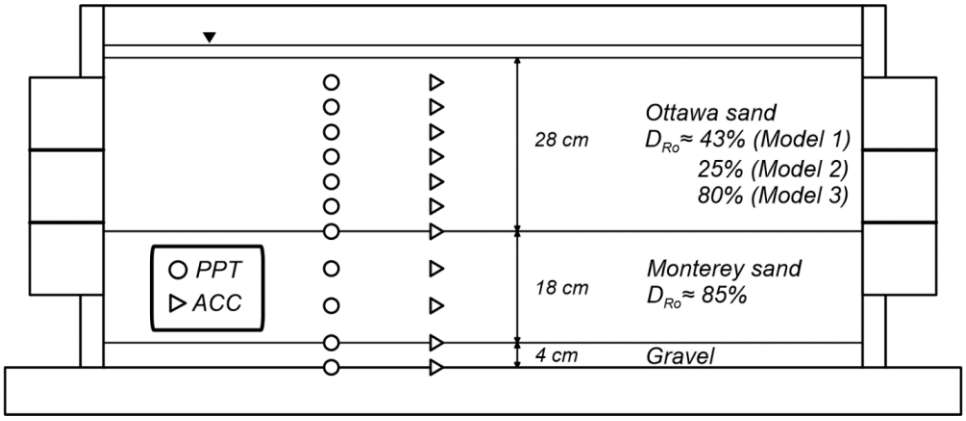

Figure 1. Centrifuge model cross section (dimensions in model scale)

Each model was subject to a series of shaking events with progressively increasing amplitudes of acceleration. Model 1 was subjected to 29 shaking events, Model 2 was subjected to 26 shaking events, and Model 3 was subjected to 17 shaking events. Each shaking event consisted of 15 cycles of a 1 Hz frequency uniform sine wave with amplitudes of acceleration ranging from 0.03 to 0.55 g. The testing sequence and select responses for Model 1 are presented in Figure 2; the testing sequences for the other two models were similar. Points are plotted against the peak base acceleration (PBA) for each shaking event. The excess pore pressure ratio ($r_u = u_e/\sigma'_{vo}$) is shown for three depths in the Ottawa sand layer: circles represent one-third depth, diamonds represent mid-depth, and triangles represent two-thirds depth. The color of the points indicates the maximum r_u generated during each event, with red points having high r_u ($r_u \geq 0.95$), open points having low r_u ($r_u < 0.70$), and yellow points having intermediate r_u ($0.70 \leq r_u < 0.95$). In-flight cone penetration tests were performed before or after select events in each model to capture progressive changes in penetration resistance resulting from the multiple shaking events. Timing of the cone penetration tests are indicated by the blue arrows across the top x-axis in Figure 2.

INVERSE ANALYSIS OF PORE PRESSURE TRANSDUCER ARRAY DATA

Profiles of volumetric strain were computed from PPT data following the procedure in Malvick et al. (2008) with the numerical smoothing function modified to account for the different boundary conditions and better fit the experimental data. Gradient and volumetric strain rate are related to excess pore pressure as:

$$i = \frac{\partial(\Delta u)}{\partial z}\frac{1}{\gamma_w} \tag{1}$$

$$\frac{\partial \varepsilon_v}{\partial t} = -\frac{k_s}{\gamma_w}\frac{\partial^2(\Delta u)}{\partial z^2} \tag{2}$$

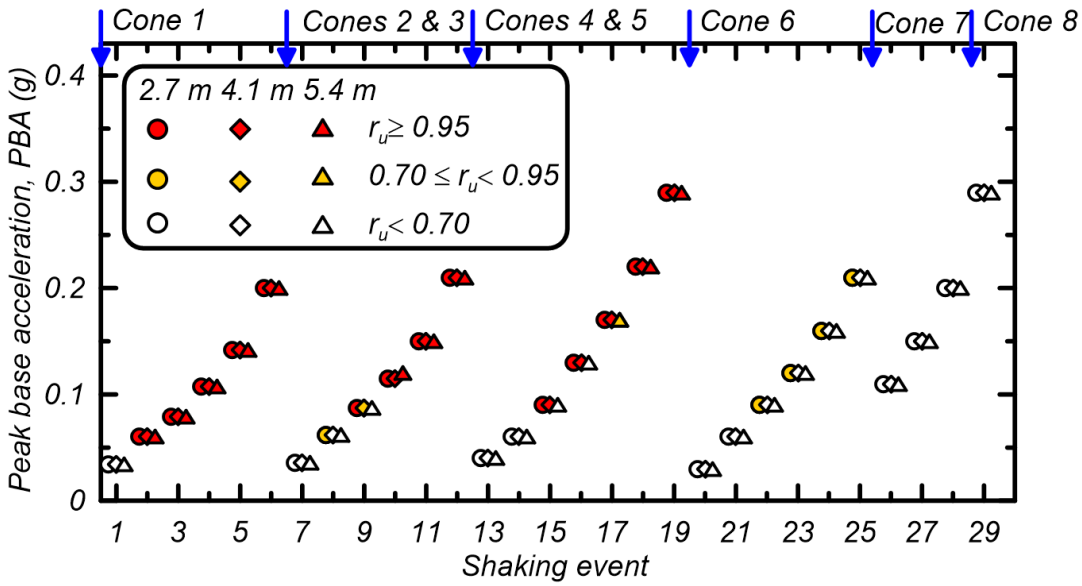

Figure 2. Time-line of shaking history for Model 1 showing peak base acceleration, peak pore pressure ratio, and timing of cone penetration tests versus shaking event number.

Prototype permeability, k in equation (2), was taken as 0.033 cm/s for Ottawa sand (data from Parra Bastidas et al. 2016) and 0.4 cm/s for Monterey sand (data from Kutter et al. 2008) based on the permeability measured with pure water times the model scale factor (40) and divided by the pore fluid viscosity scale factor (20). Profiles of volumetric strain were determined by integrating the volumetric strain rate computed in equation (2) with respect to time. Numerical smoothing of measured PPT data with respect to depth using a least-squares curve fitting procedure eliminated the high-frequency noise that can develop during differentiation of discrete data and enabled the direct differentiation and integration calculations described in equation (2). The curve fitting procedure used the functional form:

$$u_e(z) = a_0 z^6 + a_1 z^5 + a_2 z^4 + a_3 z^3 + a_4 z^2 + a_5 z \qquad (3)$$

The above functional form satisfies the boundary condition of zero excess pore pressure at the surface, and provided a better fit to the pore pressure profiles in these layered models compared to the functional form used by Malvick et al. (2008) for a uniform sand profile with an embedded silt layer. Smoothing was performed for each time step (0.008 seconds) from the start of shaking to 200 seconds after shaking ended (sufficient for full dissipation of excess pore pressures) for all shaking events (72 events total).

RESULTS OF INVERSE ANALYSES

Profiles of excess pore pressure and volumetric strain at select times for three representative shaking events are presented in Figures 3 to 5. Pore pressure isochrones from numerical smoothing

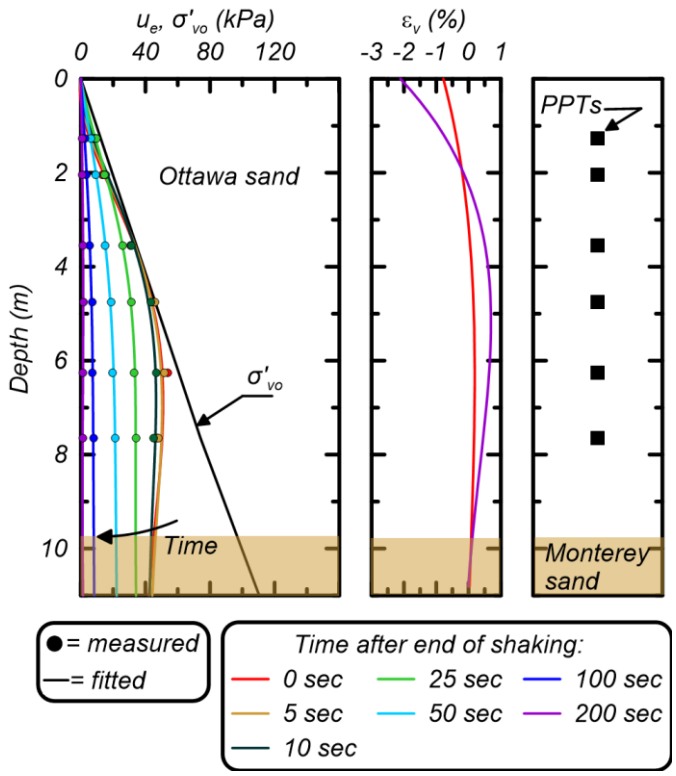

Figure 3. Isochrones of excess pore pressure and volumetric strain generation for the second shaking event (PBA = 0.06g) in Model 1 (D_{Ro} = 43%).

and measured data for the second event in Model 1, the tenth shaking event in Model 2, and the tenth shaking event in Model 1 are shown in Figures 3 to 5, respectively. These three shaking events were chosen to illustrate the range of behavior observed across all 72 shaking events. Also shown are the computed profiles of volumetric strain at the end of shaking (red curves) and at the end of dissipation (purple curves). In general, the majority of volumetric strain develops during dissipation after the end of strong shaking.

The volumetric strain profiles shown in Figure 3 (second event for Model 1; PBA of 0.06g) are representative of behavior observed early in the shaking sequence of the initially loose models. After full dissipation, negative volumetric strains (dilation or loosening) occurred in the upper 2 m with a maximum value of about 2% near the ground surface, while the rest of the profile developed less than 0.5% positive volumetric strain (contraction). Similar loosening of the upper 2 m was computed for the first six shaking events of this model. Summing the volumetric strains in the upper 2 m for the first six shaking events indicates the average D_R in the upper 2 m after the sixth event would be reduced to approximately 18% from the initial value of 43%, which is consistent with the measured reduction in cone penetration resistance over this depth interval at the same time (Darby et al. 2017).

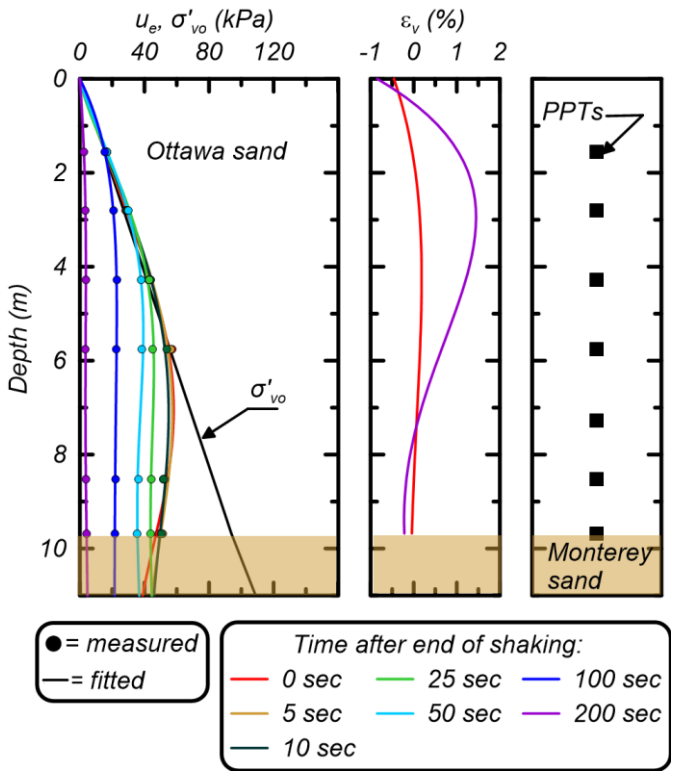

Figure 4. Isochrones of excess pore pressure and volumetric strain generation for the tenth shaking event (PBA = 0.12g) in Model 2 (D_{Ro} = 25%).

The volumetric strain profiles shown in Figures 4 and 5 (tenth events for Models 1 and 2 with PBA of about 0.12g) illustrate how the tendency for negative volumetric strains in the upper 2 m decreased as shaking progressed and the soil became denser. For this same shaking event, Model 2 (Figure 4) is still slightly looser than Model 1 (Figure 5) because it was placed initially looser. At the end of dissipation, the volumetric strain near the ground surface was about -1% (i.e., loosening) in Model 2 whereas it was about 1.3% (i.e., contraction) in Model 1. At the end of dissipation in Model 2 (Figure 4), positive volumetric strain develops towards the middle of the Ottawa sand profile, with a maximum value of approximately 1.5% at 3 m depth. Below approximately 7.5 m depth, the volumetric strain reduces to small values consistent with liquefaction not having been triggered at these depths (i.e., $r_u < 1$). At the end of dissipation in Model 1 (Figure 5) positive volumetric strains developed at all depths, with the maximum value of 1.3% occurring near the surface and strains decreasing to small values near the bottom of the Ottawa sand layer. The smaller positive volumetric strains throughout Model 1 (Figure 5), compared to Model 2 (Figure 4), are consistent with it being slightly denser and thus also developing slightly lower pore pressures and smaller peak shear strains at some depths for this same shaking motion. The pattern of volumetric strains shown for Model 1 in Figure 5 is also representative of patterns observed for many of the shaking events for the initially dense Model 3.

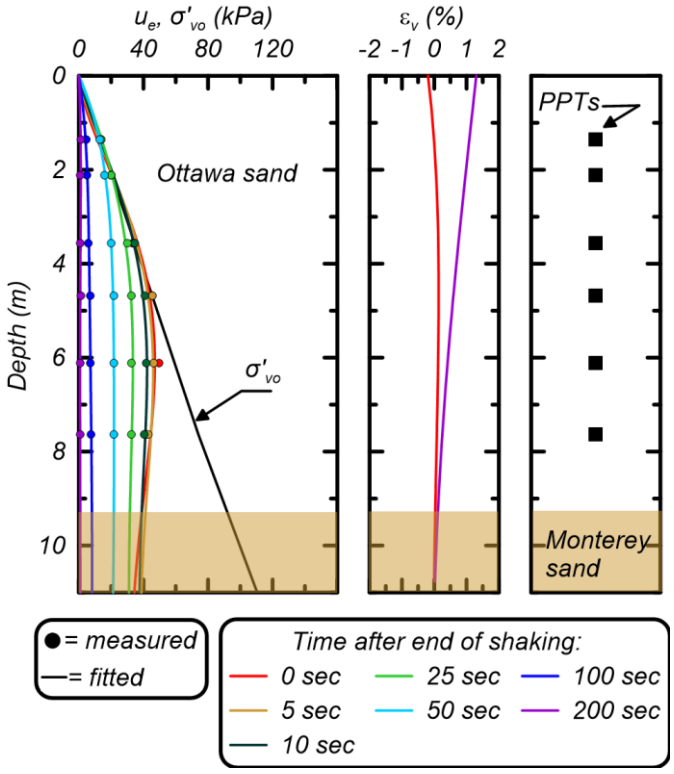

Figure 5. Isochrones of excess pore pressure and volumetric strain generation for the tenth shaking event (PBA = 0.12g) in Model 1 (D_{Ro} = 43%).

Time series of hydraulic gradient, volumetric strain rate, and volumetric strain at 2 m, 4 m, and 6 m depth in the Ottawa sand layer for the second shaking event in Model 1 (the same event shown in Figure 3) are shown in Figure 6a-c. Gradients are plotted in the top row, volumetric strain rates are plotted in the middle row, and volumetric strains are plotted in the bottom row. Data are shown from the start of shaking through 200 seconds after the end of shaking. In the plots of gradient, data are shown for a 0.2 m interval across the labeled depth; i.e., blue curves correspond to depths of 1.9 m, 3.9 m, and 5.9 m, while red curves correspond to depths of 2.1 m, 4.1 m, and 6.1 m. The graphs for volumetric strain rate and volumetric strain are for the labeled depth only. Examination of the gradients around these three depths illustrate different features of the diffusion process. At both 2 m and 4 m depth, gradients reach peak values slightly greater than unity, while gradients at 6 m reach values never exceeding 0.8; these gradients correspond to the measured PPT data shown in Figure 3, indicating liquefaction (in terms of $r_u \approx 1$) only occurs in the upper portion of the Ottawa sand. The gradients at 4.1 m and 6.1 m depths are smaller than the gradients at 3.9 m and 5.9 m depths, respectively (except briefly at 4 m depth near the start of shaking), which indicates a net outflow of pore water into these 0.2-m-thick depth intervals. The corresponding volumetric strain rates at 4 m and 6 m depths are therefore always positive, and the integrated volumetric strains are similarly always positive. The gradient at 2.1 m depth is larger than the gradient at 1.9 m depth for the first 30 seconds, but becomes smaller for all later times.

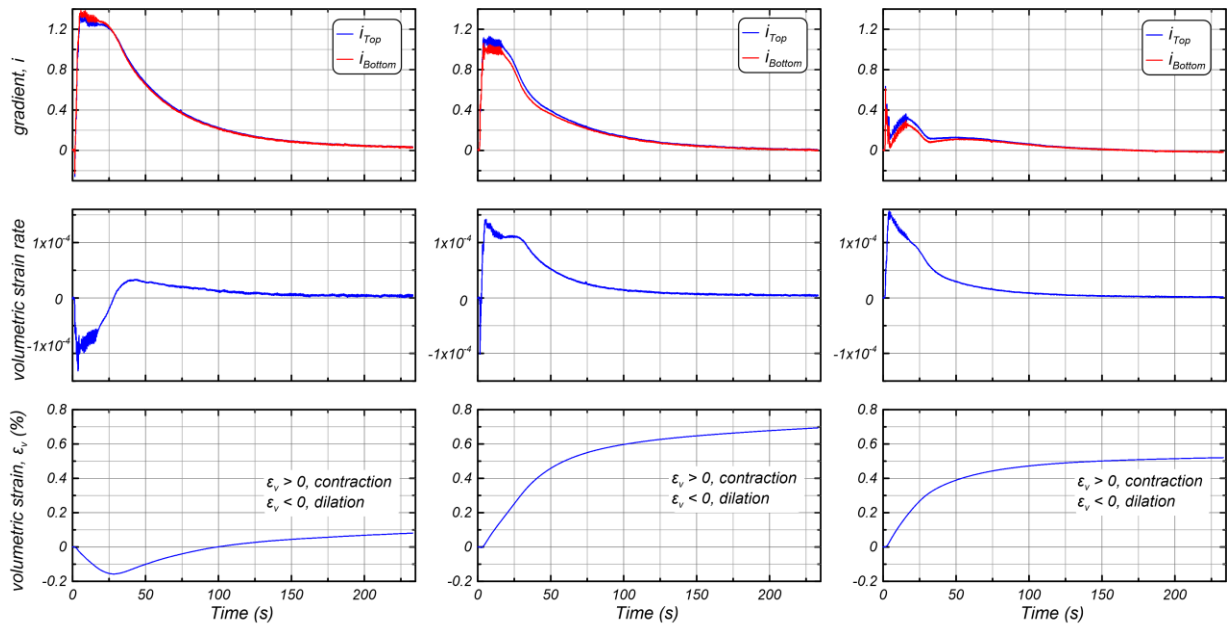

Figure 6. Time histories of hydraulic gradient, volumetric strain rate, and volumetric strain for the second shaking event in Model 1 at depths of (a) 2 m, (b) 4 m, and (c) 6 m.

The corresponding volumetric strain rate at 2 m depth is therefore negative (loosening) for the first 30 seconds, and positive afterward. The integrated volumetric strain at 2 m depth decreases to a minimum value of about -0.17% at 30 seconds, after which it progressively increases toward its final value of about 0.1% after full dissipation. The volumetric strain rates correspond to the curvature of the pore pressure isochrones in Figure 3, which consistently indicate net outflows near the middle of the model and changing inflow/outflow near the top of the model. The time histories of volumetric strain at these three depths support the observations in Figures 3 to 5 that loosening occurs primarily in the upper portion of the Ottawa sand layer and the majority of volumetric strain is generated during pore pressure dissipation.

Computed and Measured Surface Settlements

Surface settlements were computed by integration of the volumetric strains with respect to depth over the full thickness of the Ottawa sand layer. The effect of volumetric strain in the Monterey sand was not included because of limitations associated with the greater spacing between PPTs in this layer, but the additional contributions to surface settlement are not expected to be large for most shaking events because excess pore pressures were small in this lower denser layer.

The computed surface settlements are compared to surface settlements measured by LPs in Figure 7 for two times during each event: (1) the end of shaking and (2) the end of dissipation. Figures 7a-c compare computed to measured settlements at the end of shaking for models 1-3,

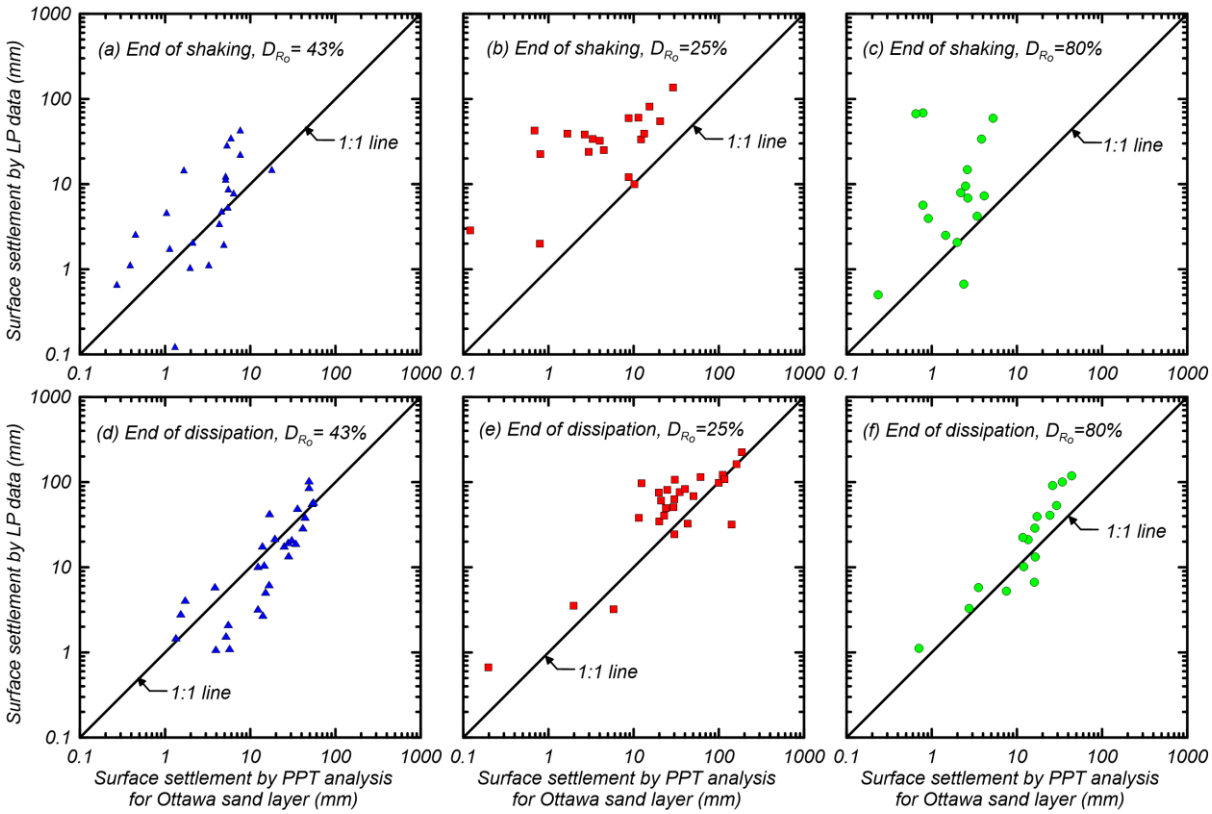

Figure 7. Surface settlements measured by LPs versus surface settlements computed by integrating volumetric strain profiles for all three models and all shaking events (top row for end of shaking; bottom row for after full dissipation).

respectively; Figures 7d-f compare computed to measured settlements at the end of dissipation for models 1 to 3, respectively. Examination of these figures indicate poorer agreement between computed and measured settlement at the end of shaking (Figures 7a-c) compared to those at the end of dissipation (Figures 7d-f).

Differences between computed and measured settlements at the end of dissipation (Figures 7d-7f) appear neither systematic nor biased by model, although computed settlements tend to be slightly lower than measured settlements for Models 2 and 3. In general, LP data is expected to indicate greater settlement because the surface settlement is influenced by volumetric strains in the underlying Monterey sand and gravel layers, whereas the computed settlements neglect their contributions. Measurements obtained during model dissection suggest the underlying Monterey sand and gravel layer contributed roughly 20% to the overall settlement measured at the surface for these three models, which is consistent with the computed settlements being smaller than the measured settlements on average.

Differences between computed and measured settlements at the end of shaking (Figures 7a-c) are more variable and show a stronger bias toward measured settlements being greater than computed settlements. Measurements of settlement during strong shaking are subject to a number

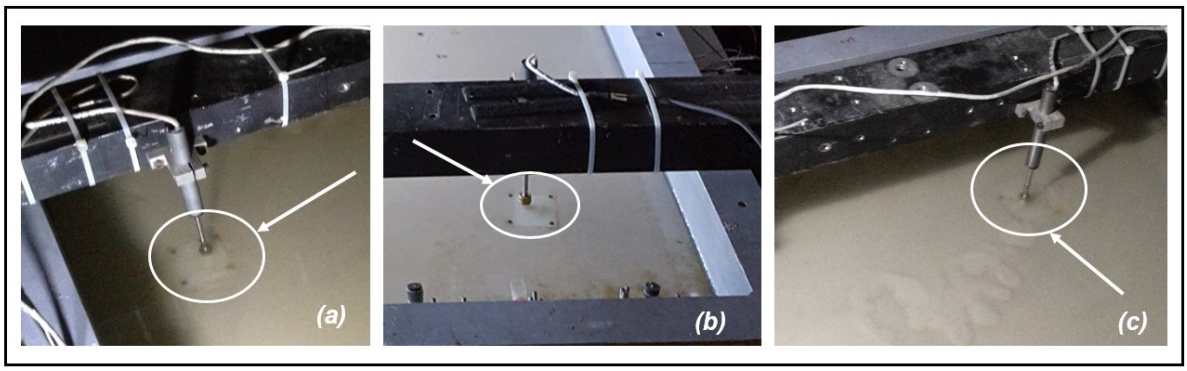

Figure 8. Examples of complications in measuring surface settlements with LPs across multiple shaking events: (a) pad tilting, (b) potentiometer sliding, and (c) pad burial.

of complications, which may contribute to these trends. LPs measure surface settlement by measuring the displacement of a metal rod whose tip is positioned in the center of a level pad resting on the soil surface. Shaking and liquefaction of the surrounding soil can cause conditions that reduce the ability of LPs to accurately measure surface settlements, including pad tilting (Figure 8a), rod sliding (Figure 8b), and pad burial (Figure 8c). An additional complication, not shown, is the potential for LP rods to "stick" when stressed laterally, resulting in noisy or unreliable settlement measurements. The above factors are expected to more strongly affect settlement measurements during strong shaking, which could contribute to both the greater scatter and bias relative to computed settlements.

Partial Drainage and Dynamic Responses

Time histories of volumetric strains, hydraulic gradients, and surfaces settlements from the inverse analyses also provide insights into the dynamic and post-dynamic responses of the Ottawa sand layer. For example, detailed responses near the middle of the Ottawa sand layer are shown in Figure 9 for the tenth shaking event (PBA of 0.12g) for Model 1; data from this event were also shown in Figure 5. Time histories during and after strong shaking are shown in the two left panels, whereas pore pressure isochrones and sensor locations are shown in the two right panels. Note the time scale on the x-axis changes between the panel for during shaking and the panel for after strong shaking. Time histories of surface settlement are plotted in the top graphs; the computed settlements (green lines) are smaller than those measured by LPs during shaking (grey lines), but fall within the range measured by LPs during dissipation. Time series for r_u, i, ε_v and acceleration are shown for the 5.0-6.0 m depth interval; i.e., the grey shaded interval in the isochrones panel, where the orange star indicates the depth, z^*, at which volumetric strain is computed (5.5 m). This shaded region was selected to investigate volumetric strain behavior between PPTs with different triggering responses. The r_u reached 1.0 at the PPT above z^* (blue line) but did not exceed about 0.8 below z^* (red line). The hydraulic gradients above z^* (blue line) is greater than below z^* (red

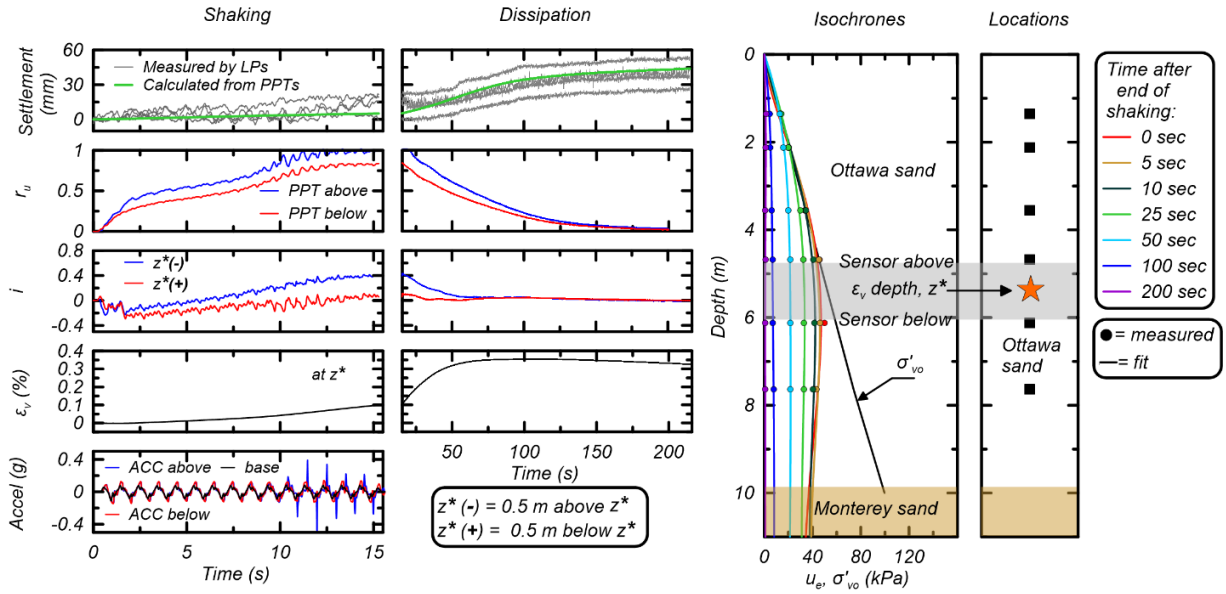

Figure 9. Response measures near the middle of the Ottawa sand layer during and after strong shaking for the tenth shaking event in Model 1.

line) for the first 75 seconds, indicating a net out-flow of pore water from this depth interval during this time. In fact, the results for the first 10 seconds of shaking show the gradient above z^* is positive (indicating upward flow) while the gradient below z^* is negative (indicating downward flow). Approximately 75 seconds after the start of shaking the gradients above and below z^* converge, indicating almost zero net flow from this depth interval. Volumetric strain at z^* indicates slight volumetric contraction during shaking (about 0.1%), increasing to a final volumetric contraction of about 0.32% after dissipation. The accelerations below z^* (red line) show minimal amplification and phase-shift relative to the base acceleration (black line), consistent with liquefaction not being triggered at or below this depth. The accelerations above z^* (red line) show high-frequency spikes and visible phase-shifts relative to the base acceleration starting approximately 10 seconds into shaking, which is consistent with the generation of $r_u = 1.0$ at this depth and time.

Volumetric Strains Prior to Triggering of Liquefaction

The time series of volumetric strain were subsequently used to determine the strains that developed prior to the triggering of $r_u = 1.0$ (i.e., $\varepsilon_{v,t}$) or throughout shaking if $r_u = 1.0$ was not generated (i.e., $\varepsilon_{v,nt}$) at each depth interval. These volumetric strains are of particular interest because they would contribute to potential increases or decreases in the liquefaction resistance of the soil at any given depth. These volumetric strains depend on the model, depth interval, and shaking event, but the results can be broadly described as follows. For cases where liquefaction is not triggered, the value of $\varepsilon_{v,nt}$ generally ranged from -0.06% and 0.11%. For cases where

liquefaction was triggered, the value of $\varepsilon_{v,t}$ generally ranged from -0.16% and 0.15%. The magnitude of these strains tends to be small when liquefaction is triggered early in shaking, simply because the time interval of pore water flow is short. The potential changes in liquefaction resistance due to these volumetric strains are currently being evaluated, and will be used to refine the correlation of the cyclic resistance ratio with cone penetration resistance from these model tests (e.g., using procedures similar to those in Darby et al. 2016, 2018).

CONCLUSION

Inverse analyses were used to evaluate the degree of partial drainage occurring during dynamic shaking of liquefying soil profiles in a set of three centrifuge model tests subjected to multiple shaking events. Non-uniform volumetric strains developed throughout the soil profiles during and after shaking. Volumetric strains during shaking were generally smaller than those during post-shaking dissipation. Surface settlements obtained by numerical integration of the volumetric strain profiles were in reasonable agreement with measured settlement values. The reasonable agreement between measured and computed settlements supports the described method for calculating profiles of gradient and volumetric strain. Examination of volumetric strains for transition zones between triggering and non-triggering behavior provide insight into the role of volumetric strain on liquefaction triggering on a system-level basis.

Future work will examine the potential changes in liquefaction resistance due to the volumetric strains that developed during strong shaking. These results will be used as part of correlating the cyclic resistance ratio with measured cone penetration resistance at different depths in these models, using procedures similar to those in Darby et al. (2016, 2018).

ACKNOWLEDGEMENTS

This material is based upon work supported by the National Science Foundation (NSF) under grants CMMI-1300518 and CMMI-1635398. Operation of the centrifuge facility at the University of California at Davis was supported as part of the Natural Hazards and Engineering Research Infrastructure (NHERI) network under NSF award CMMI- 1520581. Any opinions, findings, and conclusions or recommendations expressed in this material are those of the authors and do not necessarily reflect the views of the National Science Foundation. The authors appreciate the assistance of the staff of the Center for Geotechnical Modeling at UC Davis.

REFERENCES

Darby, K. M., Boulanger, R. W., DeJong, J. T., and Bronner, J. D. (2018). "Progressive changes in liquefaction and cone penetration resistance across multiple shaking events in centrifuge tests". Journal of Geotechnical and Geoenvironmental Engineering, ASCE, [In review].

Darby, K. M., Boulanger, R. W., and DeJong, J. T. (2017). "Effect of multiple shaking events on cone penetration resistances in saturated sand." Proc., Performance-based Design in Earthquake Geotechnical Engineering, PBD-III Vancouver, M. Taiebat et al., eds., ISSMGE Technical Committee TC203, paper 534.

Darby, K. M., Bronner, J. D., Parra Bastidas, A. M., Boulanger, R. W., and DeJong, J. T. (2016). "Effect of shaking history on cone penetration resistance and cyclic strength of saturated sand." Proceedings, Geotechnical and Structural Engineering Congress, Phoenix, AZ, Feb. 14-17, ASCE, 1460-1471.

Howell, R., Rathje, E. M., Kamai, R., and Boulanger, R. W. (2012). "Centrifuge modeling of prefabricated vertical drains for liquefaction remediation." Journal of Geotechnical and Geoenvironmental Engineering, ASCE, 138(3), 262-271.

Kamai, R., and Boulanger, R. W. (2010). "Characterizing localization processes during liquefaction using inverse analyses of instrumentation arrays." Meso-Scale Shear Physics in Earthquake and Landslide Mechanics, Y. H. Hatzor, J. Sulem, and I. Vardoulakis, eds., CRC Press, 219-238.

Kutter, B. L., Chou, J.-C., and Travasarou, T. (2008). "Centrifuge testing of the seismic performance of a submerged cut-and-cover tunnel in liquefiable soil." Geotechnical Earthquake Engineering and Soil Dynamics IV, GSP 181, ASCE.

Malvick, E. J., Kutter, B. L., Boulanger, R. W. (2008). "Postshaking shear strain localization in a centrifuge model of a saturated sand slope". *Journal of Geotechnical and Geoenvironmental Engineering*, ASCE 132(2), 164-174.

National Research Council (NRC) (1985). Liquefaction of Soils During Earthquakes, National Academy Press, Washington, DC, 240 pp.

Parra Bastidas, A. M., Boulanger, R. W., Carey, T. J., DeJong, J. T. (2016). "*Ottawa F-65 sand data from Ana Maria Parra Bastidas"*, NEEShub, http://dx.doi.org/10.17603/DS2MW2R.